DETECTION OF REVERSAL OF THE MAGNETIC FIELD OF THE SUN IN SNOWFALL RECORDS IN THE SIERRA, ROCKY, AND CASCADE MOUNTAIN RANGES OF THE WESTERN UNITED STATES.

John A. Kleppe[1*] and Daniel S. Brothers[2]

ABSTRACT

The major driving forces of winter precipitation, in the form of snow, in the Sierra, Rocky, and Cascade mountain ranges are shown in this paper to be the reversal of the sun's magnetic field and a statistically independent "carrier" signal being generated by the Earth's large-scale atmospheric circulation parameters. We present wavelet analyses of several long-term Snow Water Equivalent (SWE) records from the Sierra, Rocky, and Cascade mountain ranges and found linkages between sunspots (i.e., the magnetic activity of the sun), and SWE. It is important to note the 11 year and 22-year visible sunspot cycles are **NOT** found in the SWE data, but rather, we found evidence of a Sun-Earth magnetic carrier suppressed amplitude modulation system that modulates the formation of the snowpack resulting in the generation of signals detected in the SWE records. The ISSN data were selected to match the Water Year (1 October to 31 March) and signed to account for the magnetic polarity of the sunspots. It is important to note the **magnetic cycle** of the sun is not 11 years but rather it requires the sum of two sunspot cycles, which is approximately 22 years, to return to its original magnetic polarity. The resulting ISSN series was demodulated using suppressed carrier amplitude modulation methods and correlated to the corresponding SWE series. The correlation coefficient amongst each of the stations in similar climate regions is surprisingly high, which suggests SWE variation is regionally correlated and that each of these sites experiences the same forcing function. The resulting comparison suggests the "footprint" of the sun is detected in the SWE data; and, it appears to be a forcing mechanism in the drought cycle of the Sierra, Rocky, and Cascade mountain ranges in the western United States. (KEYWORDS: snowpack, sunspots, solar magnetic reversal, rotational, cosmic).

INTRODUCTION

Snowpack, in the Sierra, Rocky and Cascade mountain ranges, provides a natural form of water storage which greatly impacts the economies of the western United States. (Kleppe & Brothers, 2017) concluded the major driving forces of winter precipitation, in the form of snow, in the northern and central Sierra, Figure 1, are the reversal of the sun's magnetic field; and, a statistically independent "carrier" signal being generated by the Earth's atmospheric circulation parameters.

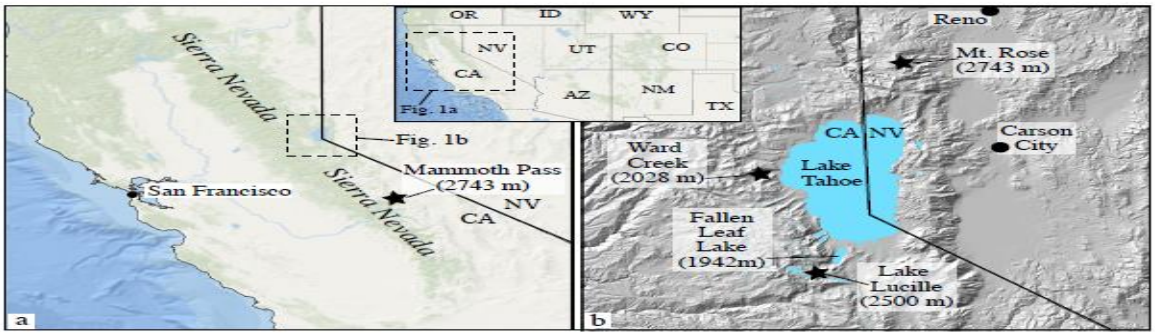

Figure 1. (**a**) Regional setting. (**b**) Enlarged map of the Lake Tahoe Basin and surrounding terrain. Snow Water Equivalent sites (SWE) from (Kleppe & Brothers, 2017) are labeled as black stars.

The authors also reported the snowpack variability in the northern and central Sierra is not only a function of individual watersheds and/or local topographic relief, but is to a larger degree, a function of broad-scale climatic phenomena affecting the entire Sierra Nevada mountain range. The snowpack in the Rocky and Cascade mountain

Paper presented Western Snow Conference 2018
[1]John A. Kleppe, College of Engineering, University of Nevada, Reno, NV 89557-0260, Kleppe@unr.edu
[2]Daniel S. Brothers, Pacific Coastal and Marine Science Center, U.S. Geological Survey, Santa Cruz, CA.95060

ranges, like the Sierra Nevada, have a major impact on the economies of the areas serviced by their respective watersheds. In this paper, we extend the results of our investigation for the northern and central Sierra Nevada, (Kleppe & Brothers, 2017), to the southern Sierra and to the Rocky and Cascade mountain ranges, shown in Figure 2. The site locations and details of the snowcourse sites (shown as yellow pins) selected for this paper are listed in Table 1.

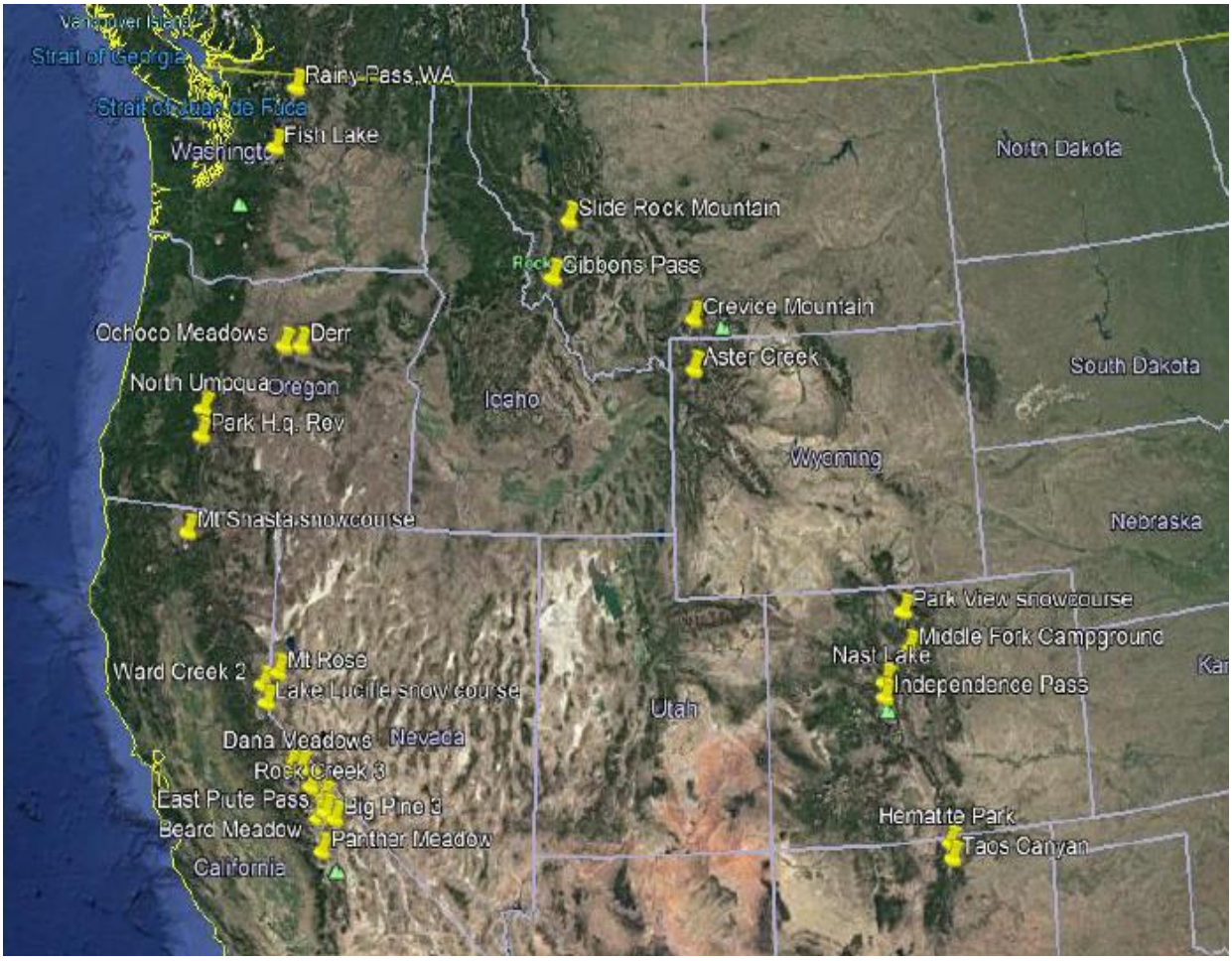

Figure 2. Map of the areas of the Sierra, Cascade, and Rocky mountain ranges reported in this paper. Snow Water Equivalent sites (SWE) are labeled with yellow pins.

The generation of precipitation involves many complex and interrelated factors; however, it has been reported, (Kleppe & Brothers, 2017) on how this complex system can be modeled using a suppressed carrier amplitude modulation process. This technique involves the multiplication of three signals, the first being an Earth statistically independent "carrier" signal, f_c, being generated by the Earth's large-scale atmospheric circulation parameters, the second, the Annual Corrected Water Year Sun Spot Number (ACWYSSN), f_s and the third, the amplitude of the sunspot cycle referred to as the Gleissberg Cycle (GC) f_g.

DATA AND METHODOLOGY

Kleppe & Brothers (2017) investigated, using wavelets, several long-term Snow Water Equivalent (SWE) records in the northern and central Sierra Nevada and found linkages between sunspots (i.e., the magnetic activity of the sun) and SWE. It is important to note the 11-year and 22-year visible sunspot cycles are **NOT** found in the SWE data, but rather, we found evidence of a Sun-Earth magnetic carrier suppressed amplitude modulation system that modulates the formation of the Sierra snowpack resulting in the generation of four signals. This paper is an extension of our work to include SWE records located in the southern Sierra, Rocky, and Cascade mountains.

Table 1. Site location information for the snowcourse sites shown in Figure 2

Region/site name	Station ID	Location LAT/LONG	Elevation (m)	Climate region	Period of data	Correlation with first listed in Region
Sierra mountains						
Lake Lucille	20L04	38.86/-120.11	2,495	CA-3	1913-2017	1.00
Beard Meadow	BMD	37.11/-118.84	2,987	CA-7	1930-2017	0.86
Big Pine Creek 3	BP3	37.13/-118.47	2,987	CA-5	1926-2017	0.69
Dana Meadows	DAN	37.90/-119.26	2,987	CA-3,5	1927-2017	0.88
East Piute Pass	EPP	37.23/-118.69	3,292	CA-5	1930-2017	0.83
Mammoth Pass	MAM	37.61/-119.03	2,835	CA-3,5,7	1928-2017	0.90
Mt Rose	19KO2	39.35/-119.88	2,743	NV-1	1910-2017	0.88
Mt Shasta	MSH	41.37/-122.23	2,408	CA-1,2	1930-2017	0.69
Panther Meadow	PTM	36.59/-118.72	2,621	CA-5	1925-2017	0.75
Rock Creek 3	RC3	37.45/-118.74	3,048	CA-5,7	1928-2017	0.81
Snow Flat	SNF	37.83/-119.50	2,652	CA-5	1930-2017	0.89
Ward Creek 2	20K17	39.14/-120.22	2,134	CA-3	1913-2017	0.88
Cascade mountains						
Park H.q. Rev	22G05	42.90/-122.14	2,003	OR-3,5	1945-2017	1.00
Fish Lake	21B04	47.53/-121.09	1,006	WA-5,6	1943-2017	0.67
Derr	19E03	44.45/-119.93	1,786	OR-7	1937-2017	0.70
North Umpqua	22F16	43.31/-122.16	1,280	OR-7	1937-2017	0.68
Ochoco Meadows	20E02	44.43/-120.34	1,582	OR-7	1935-2017	0.68
Rainy Pass	20A09	48.52/-120.74	1,457	WA- 5,6	1936-2017	0.50
Rocky mountains						
North						
Aster Creek	10E08	44.27/-110.63	2,362	WY-2	1937-2017	1.00
Crevice Mt.	10D05	45.04/-110.61	2,560	MT-5	1935-2017	0.69
Gibbons Pass	13D02	45.70/-113.94	2,164	MT-1,2	1939-2014	0.87
Slide Rock Mt.	13C02	46.59/-113.57	2,164	MT-1	1937-2017	0.74
Middle						
Independence Pass	06K04	39.07/-106.62	3,231	CO-2	1936-2017	1.00
Middle Fork Campground	06K12	39.78/-106.02	2,743	CO-2	1936-2017	0.57
Nast Lake	06K06	39.30/-106.60	2,652	CO-2	1936-2017	0.64
Park View	06J02	40.37/-106.10	2,792	CO-2,4	1936-2017	0.66
South						
Hematite Park	05N03	36.67/105.37	2,896	NM-2	1937-2017	1.00
Taos Canyon	05N02	36.41/-105.33	2,774	NM-2	1939-2017	0.85

Snow Water Equivalent (SWE) data in the Sierra, Rocky, and Cascade mountains

From 1905 to 1915 the pioneer of snow sampling, Professor J.E. Church of the University of Nevada, Reno, invented a snow pack sampling methodology and established a system of snow courses at Mt. Rose and within the Lake Tahoe Basin, Figure 1. Since that time, hundreds of snow course sites have been established and are maintained throughout the western United States, https://www.wcc.nrcs.usda.gov/snow/ . We selected representative sites based mainly on their locations and the length of records. For example, the SWE recorded at Mt Rose (19K02) in the Sierra is one of the longest continuous SWE records available (1910-2017) in the United States.

Spectral Analysis

Among all the spectral analysis tools used in frequency analysis, the most commonly applied is the Fourier transform. Although the Fourier transform is efficient and robust for analyzing the frequency content of a periodic signal over an entire time record, it is limited in its ability to detect changes in frequency as a function of time. The Morlet Wavelet transform, on the other hand, can capture the short duration, high frequency, as well as the long duration, low frequency information simultaneously (Torrence & Compo, 1998). For example, Figure 3, shows the

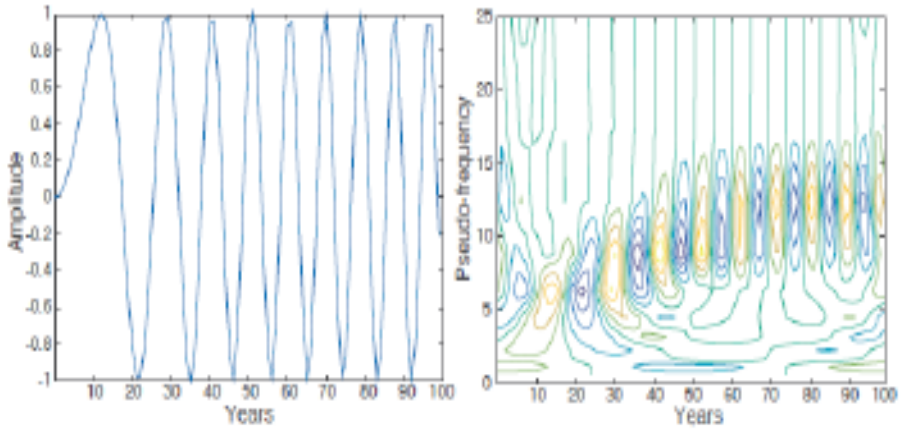

Figure 3. Example of a frequency modulated sine wave defined as y = (sin(2*pi*0.1*t.*k)) and k=(1.0-exp(-t*0.02)) and application of the Morlet Transform.

Morlet Transform is applied to a known time varying periodic signal where it becomes straightforward to observe the time-varying frequency content. Data were analyzed using both Fourier Transform and Morlet Wavelet Transform methods. The data were de-trended and passed through an anti-aliasing, second-order Butterworth low-pass filter with a cutoff period of 3.3 years. The sampling rate was chosen to satisfy the Nyquist rate of at least 2 times the highest frequency content in the data records. Because the data have relatively few samples (~100 measurements or less), it was necessary to apply a Hamming window prior to applying the short record FFT and/or the Morlet Transforms. Furthermore, the frequency (or period) resolution is relatively coarse since resolution is a function of the inverse of the time record length.

Sunspots Solar Cycles, and the Gleissberg Cycle during the Water Year (October 1 to March 31)

We used the revised Version 2.0 monthly International Sun Spot Number (ISSN) data for our analysis from the World Data Center SILSO, Royal Observatory of Belgium, Brussels**.** The ISNN record is divided into 24 cycles starting with Solar Cycle #1 beginning in 1755 and continuing up to the present Solar Cycle 24

The first step in our analysis was to reconstruct the ISSN monthly time series data to account for the reversal of the sun's magnetic field every 11 years. This procedure resulted in a modified sunspot record with a Solar cycle period of approximately 22 years (two conventional sun cycles).

The traditional ISSN time series was then converted from calendar year to Water Year to match the timing of the Sierra Nevada snowpack measurements (October 1st to March 31st). We denote the modified series as ACWYSSN. As with the SWE data, the ACWYSSN time series was analyzed using the same Fourier and Morlet Wavelet Transform methods described earlier.

Numerous authors over many years have noted there are multi-cycle periodicities in the sunspot cycle amplitudes. Gleissberg in1939 first noted a periodicity of seven or eight 11-year solar cycles (77 to 88 years) in the cycle amplitudes from 1750 to 1928 (Gleissberg, 1967). These amplitude variations of the solar cycles have since become known collectively as the Gleissberg Cycle (GC) (Feynman & Ruzmalkin, 2014). The apparent complex period variation of the GC (sunspot amplitudes) explains why so many different results for the period of the GC have been reported over the years. We used an appropriate curve fitting routine to determine a time variable curve fit for the GC, which has a correlation coefficient of 0.72 (Kleppe & Brothers, 2017). We use the resulting time series as the GC signal, fg, for our analysis.

Cosmic Rays and the Possible Formation and Seeding of Clouds on Earth

Galactic Cosmic Rays (GCRs) are energetic particles coming from outside the solar system. There have been numerous papers published over many years describing the anti-correlation between sunspot numbers (magnetic activity of the sun) and the modulation of GCRs. The role of ionization in atmospheric processes by GCRs has been a controversial matter since it was first suggested fifty years ago. The cosmic rays are thought to affect cloud formation on Earth by creating condensation nuclei, Kleppe & Brothers (2017), Yu and Luo (2014), and

Svensmark et al. (2017) have recently provided additional support for the inferred linkages between cosmic rays and clouds on Earth. They propose the Sun's changing magnetic field has an influence on GCRs, with a stronger magnetic field deflecting more cosmic rays and a weaker one allowing more into the solar system.

An Amplitude Modulation Model for the Generation of SWE.

The mathematical basis of our model is described in (Kleppe & Brothers, 2017). In words, our hypothesis is, the snowpack (SWE) in the Sierra, Rocky, and Cascade mountains is being created by a carrier suppressed amplitude modulation process involving the multiplication of three signals, the first being a statistically independent "carrier" signal, f_c, being generated by the Earth's atmospheric circulation parameters including orbital (inclination, eccentricity, precession, obliquity, and rotational), depth of the atmosphere, and heating by the sun; the second signal, f_s, being generated by the frequency of the reversal of the sun's magnetic field; and, the third signal, f_g, being due to the time varying amplitude of the sun's magnetic field represented by GC. It is noted, in the above process, the multiplication of the three signals of frequency fc, fs and fg results in the generation of four signals which we will denote as f_1, f_2,f_3,and f_4.

It is possible to arrange these operations in the tabular form shown below for easy analysis. The T_n are the respective periods calculated as the inverses of each f_n:

$$\begin{aligned} f_{1=1/T1} &= fc + fs + fg \\ f_{2=1/T2} &= fc + fs - fg \\ f_{3=1/T3} &= fc - fs + fg \\ f_{4=1/T4} &= fc - fs - fg \end{aligned} \qquad [1]$$

The Earth carrier frequency is not separately present in the carrier suppressed modulated signal. The solution of equation [1] provides a starting value for fc in our modulation model. We first multiply fc times the modified sunspot record ACWYSSN, and then multiply this product by the time series GC. The result of this multiplication produces an estimated value, SWEe. The model then calculates the cross-correlation coefficient between the measured values, SWEm, and the estimated values, SWEe, and applies iteration methods to adjust the model parameter f_c, to maximize the correlation coefficient.

RESULTS

We compared in our previous paper, (Kleppe & Brothers, 2017), the spectral content from several spatially separated Sierra Nevada snow course sites. The Lake Lucille (20l04) sampling site and the two other nearby sites, Ward Creek #2 (20K17) and Mt. Rose (19K02), were selected as representative sites for the Lake Tahoe region. The fourth site, farther south, was established in 1928 at Mammoth Pass (LADWP-205). The Mammoth Pass snow course provided a continuous 86-year record from a more distant location, but still within the same U.S. Climate Division as the other three sites (Nevada 1 and California 3), (Russel et al, 2014). Cross correlation estimates yielded correlation coefficients of 0.88 suggesting the SWE spectral content was highly correlated over a broad area of the northern to central Sierra Nevada.

The spectral calculations for the water year period 1928 to 2014 revealed a nearly identical peak period of 14.5 years, and a second peak at a period of ~32 years, a third peak with a period of 7.9 and a fourth more subtle peak at a period of ~6 years for the four Sierra Nevada SWE sites. The longer record of SWE data for the period 1913 to 2014 at Lake Lucille, Ward Creek, and Mt. Rose showed the four peaks more clearly. The use of the Morlet transform allowed us to observe the shift in the 14.5-year period in the SWE data that was not observable using standard FFT analysis. It is very important to note the spectral shift of the major "drought buster" (El Niño) peak shown in the wavelet record. The peak period shifted from 16 years to 12 years over the 91year SWE data record from 1916 to 2007. This is a period shift of approximately 0.044 years per year being generated by the time variable Gleissberg Cycle. The average period between the El Niño peaks is therefore getting shorter meaning more frequent Atmospheric Rivers are to be expected during upcoming winters.

Snowcourse sites located in the southern Sierra, Rocky and Cascade mountains with long historical records were added, as shown in Table 1, and investigated using our same approach. The analysis of SWE data from these additional snowcourse sites show solar forcing on SWE records, but with different carrier frequencies, f_c. The results of this extended investigation are reported below.

Ocean Atmospheric Interactions and Formation of the Sierra, Rocky, and Cascade Mountain Snowpack

Ocean-atmospheric interactions normally considered when looking at origins of winter precipitation forming the Sierra, Rocky, and Cascade mountain snowpack are the Pacific/North American teleconnection pattern (PNA), the El Niño–Southern Oscillation (ENSO), and the Pacific Decadal Oscillation (PDO), (Oakley & Redmond, 2014).

Cayan (1996) studied six decades of snow course records over 11 western states and found 1 April snow water content (SWE) variations showed regional spatial coherence driven by large scale atmospheric circulation over the North Pacific/North American area. Cayan concluded anomalies of SWE are quite sensitive to the large-scale atmospheric circulation. The extended PNA index has been compared with indices of the North Atlantic Oscillation, the PDO, and the ENSO and the relationship to these indices was found to be stationary over the past century (Ewen et al., 2008; Bronnimann et al., 2009).

The PNA, from http://www.cpc.noaa.gov/data/teledoc/pna.shtml, is one of the most prominent modes of low-frequency variability in the Northern Hemisphere extratropics. The positive phase of the PNA pattern features above-average heights near Hawaii and over the intermountain region of North America, and below-average heights located south of the Aleutian Islands and over the southeastern United States. The PNA pattern is associated with strong fluctuations in the strength and location of the East Asian jet stream. Figure 4 presents the spectral record of the PNA winter (DJFM) index from (Liu, et al, 2017) and personal communications.

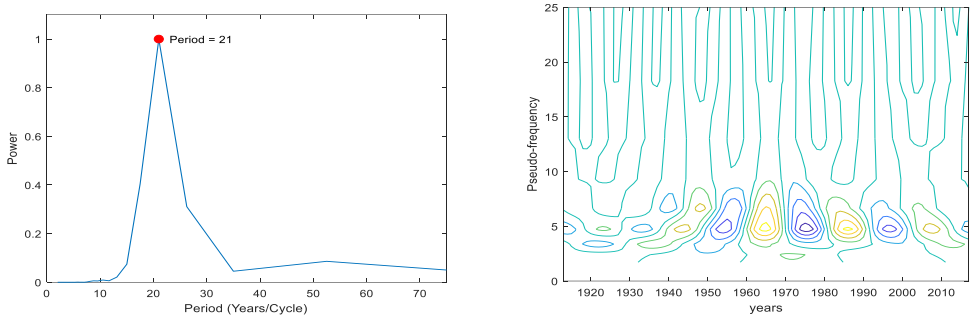

(a)

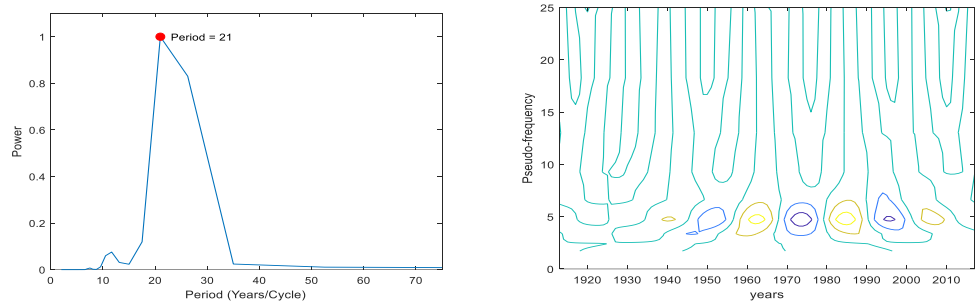

(b)

Figure 4. Comparison of spectral results for the winter PNA index for the period 1913 to 2017, (a) Actual WYPNA index. (b) Model output with ρ= 0.71.

The ENSO, from http://origin.cpc.ncep.noaa.gov/products/analysis_monitoring/ensostuff/ONI_v5.php , is the name given to the cycle of warm and cold temperatures, as measured by sea surface temperature (SST) of the tropical central and eastern Pacific Ocean The Oceanic Niño Index (ONI) has become the de-facto standard that NOAA uses for identifying El Niño (warm) and La Niña (cool) events in the tropical Pacific. It is interesting to investigate, using our model, the most recent running 3-month mean sea surface temperature (SST) data available for El Niño (warm) and La Niña (cool) in the Niño 3.4 region i.e., 5ºN-5ºS, 120º-170ºW.

Figure 5 presents a comparison between the spectral content of the ONI converted to WY and the spectral content of the Mt. Rose SWE data over the period WY1951 to WY2016. It is clear a similar spectral response is seen and suggests the El Nino may be driven by the same Sun-Earth modulation process.

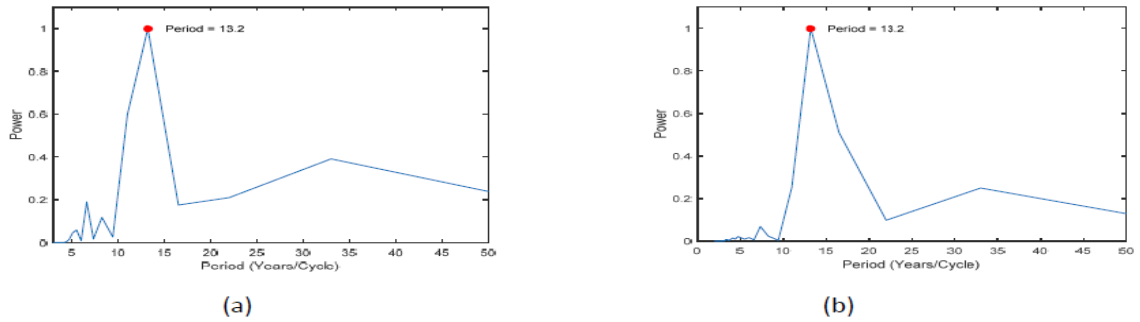

Figure 5. Spectral record of (a) MT. Rose SWE and (b) the Oceanic Niño Index (ONI) from WY 1951 to WY 2016.

The PDO, from **https://www.ncdc.noaa.gov/teleconnections/pdo/,** is the dominant year-round pattern of monthly North Pacific SST variability and is the subject of much ongoing research to understand the process. Research has determined the PDO may not be a single physical mode of climate variability but instead may largely represent the combination of three groups of processes involving the Aleutian low, El Nino, oceanic memory, or thermal inertia, and decadal changes in the Kuroshio-Oyashio system, (Jia & Ge, 2017), (Newman et al., 2016). The PDO is often described as a long-lived El Nino-like pattern of Pacific climate variability (Zhang et al., 1997), (Matua & Hare, 2002).

We used the monthly NCEI PDO index data available from NOAA. The data set covers the period 1854 to 2017. The monthly data were converted to the water year of October 1 to March 31st and the wavelet spectrum is shown in Figure 6 for the period 1913 to 2017. The four most dominant spectral peaks are seen to be T1=7.286, T2=9.273, T3=20.400, and T4=51.00. In frequency these values are f1= 0.13725, f2=0.10784, f3=0.04902, and f4=0.01961. Using equation (1), the original three periods are found to be Tc=12.8, Ts= 22.7, and Tg=68.0. We then used the starting value Tc= 12.75, from equation (1), to reconstruct the NCEI WYPDO index from the multiplication of the carrier period, Tc=12.75, the water year sunspot data ACWYSSN, Ts, and the Gleissberg Cycle, Tg. The results of this multiplication using our model are shown in Figure 6. The correlation between the actual NCEI PDO and the model output for this example is ρ= 0.62.

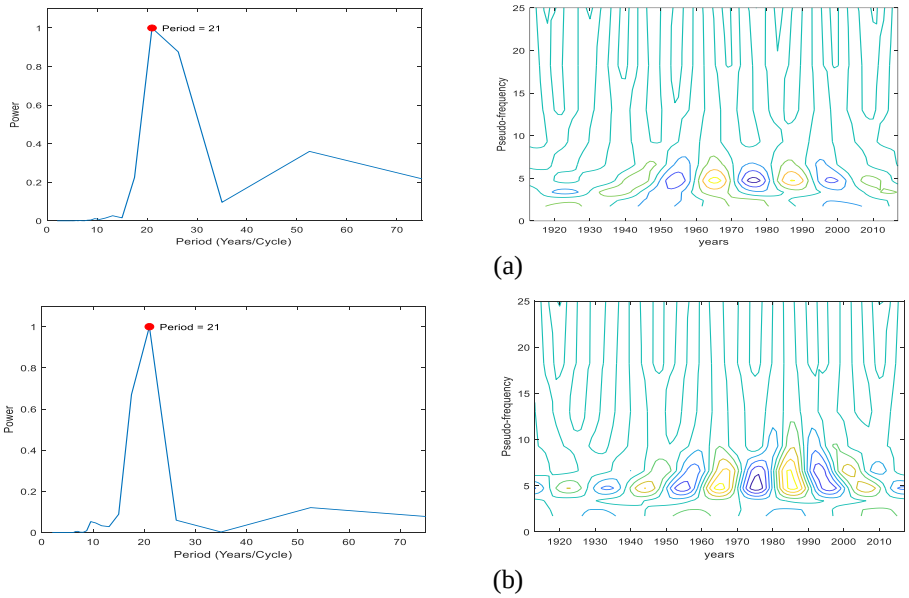

Figure 6. Comparison of spectral results for the NCEI PDO water year data for the period WY1913 to 2017, (a) Actual WYPDO data. (b) Model output with ρ= 0.62.

This analysis suggests the WYPDO is also being generated by the same amplitude modulation process as is seen in the SWE data and the PNA and ENSO spectral records. Examples are shown below for typical snowcourse sites in the Sierra, Cascade, and Rocky mountain ranges demonstrating how our model works for the areas listed in Table 1.

Sierra Nevada mountains

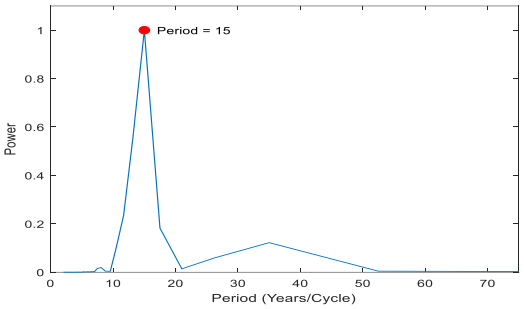

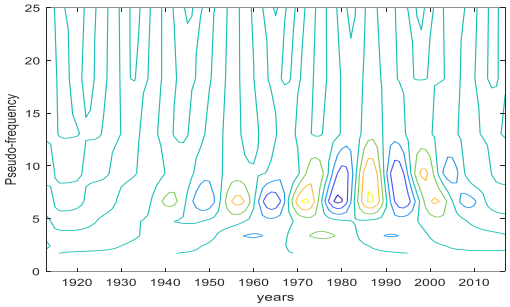

(a)

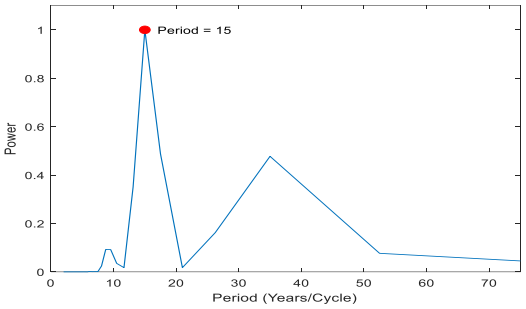

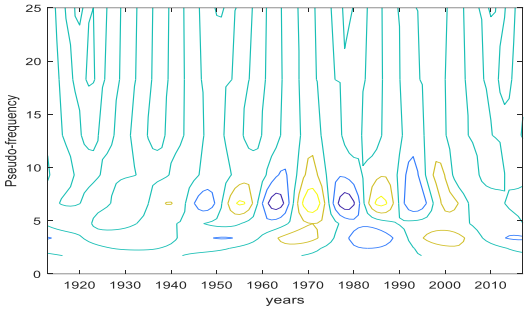

(b)

Cascade mountains

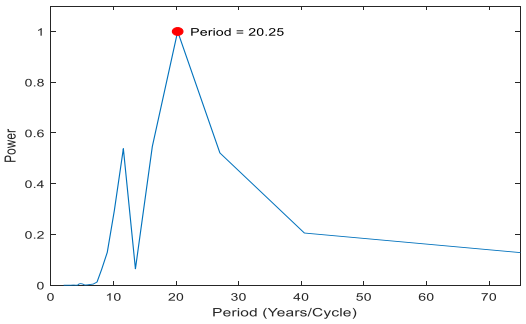

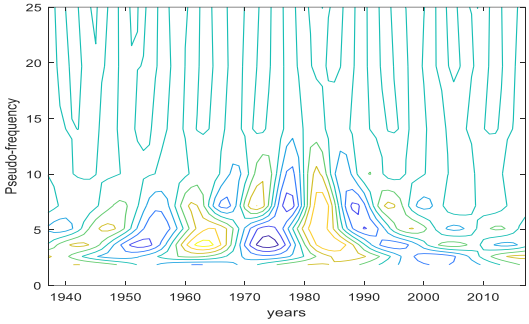

(c)

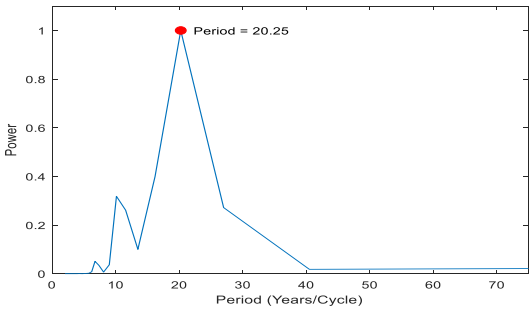

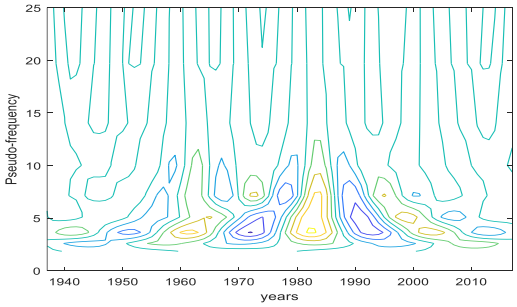

(d)

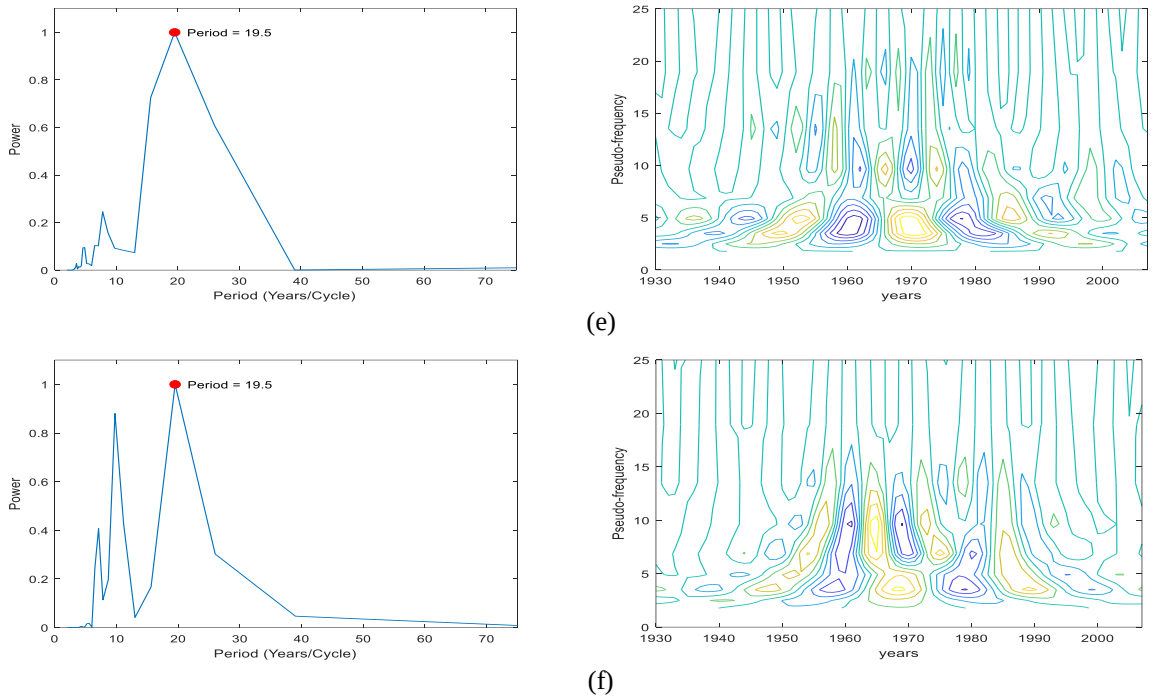

Figure 7. Comparison of spectral results for typical sites located in the Sierra, Cascade, and Rocky Mountains, (a) Actual SWE data from Sierra, Lake Lucille(20L04) 1913 to 2017 (b) Model output for (a) with ρ=0.67. (c) Actual SWE from Cascades, North Umpqua(22F16) 1937 to 2017. (d) Model output for (c) with ρ= 0.74. (e) Actual SWE data from Rockies, Aster Creek(10E08) 1930 to 2007. (f) Model output for (e) with ρ= 0.60.

DISCUSSION AND CONCLUSIONS

The correlations between the WYPNA, WYENSO, WYPDO indices and our model outputs are high. This indicates the PNA, ENSO, and PDO appear to be driven by the magnetic reversal of the sun. The mechanism may be the wide area modulation of cloud cover over the Pacific Ocean by variations in the cosmic ray flux. It is important to note a mixture of the WYPNA, WYENSO, and WYPDO spectral frequencies do appear in the SWE records.

The spectral content of the SWE data and the high correlation coefficients amongst the sites located in each of the mountain regions, listed in Table 1.0 suggests Sierra, Rocky, and Cascade mountain snowpack variability are not only a function of individual watersheds and/or local topographic relief, but are also a representation of broad-scale climatic phenomena affecting each of the mountain ranges.

The generation of precipitation falling onto the Sierra, Rocky, and Cascade mountains involves many complex and interrelated factors; however, it is interesting to see how these very complex systems may be lumped into a simple model. The process can be modeled using a suppressed carrier amplitude modulation process. This involves the multiplication of three signals, the first being an Earth statistically independent "carrier" signal, fc, being generated by the Earth's large scale atmospheric circulation parameters, the second, the Water Year modified sunspot cycle, fs , and the third, the Gleissberg Cycle, fg. It is important to note the Earth's carrier signal remained stationary for each of the areas over each of the periods of our analysis which supports the idea that large scale atmospheric circulation remains stationary in the areas we studied.

It is important to note in the Sierra mountains the quasi-periodic function with a wavelength of 14 to 15 years reported by St. George & Ault (2011), without a physical mechanism to explain the presence of the rhythm; and, the approximate average "drumbeat "of the 15-year period in the 60-year data record, cited by (Dettinger and Cayan, 2014), is the variable peak period we found in the highly correlated SWE data analyzed from Table 1 and

shown in Figure 7. We conclude the "drought buster" El-Niño cycle is changing to a shorter period in response to changes of the Gleissberg Cycle at a rate of approximately 0.044 years per year.

We feel it is highly likely the anti-correlation GCRs may be the mechanism responsible for the connection between the magnetic activity of the sun (sunspots) and the SWE.

Based on the results presented in this paper, we conclude the major driving forces of winter precipitation, in the form of snow, in the Sierra, Rocky, and Cascade mountains are the reversal of the sun's magnetic field; and, a statistically independent "carrier" signal being generated by the Earth's large-scale atmospheric circulation parameters.

This work can be extended to include the study of past droughts by reconstructing the sunspot record accordingly.

ACKNOWLEDGEMENTS

The WDC-SILSO, Royal Observatory of Belgium, Brussels for use of their data bank for our sunspot numbers.

Professor Zhongfang Liu of the State Key Laboratory of Marine Geology, Tongji University, Shanghai, China, the Atmospheric and Ocean Research Institute, University of Tokyo, Japan, and the Department of Earth Sciences, University of Southern California, CA, USA for providing us with the extended PNA data.

REFERENCES

Bronnimann, S., et al. 2009. Variability of large-scale atmospheric circulation indices for the northern hemisphere during the past 100 years, Meteorogische Zeitschrift, Vol.18 No. 4, 379-396.

Cayan, D. R. 1996. Interannual climate variability and snowpack in the Western United States, Journal of Climate, Vol.9, 928- 948.

Dettinger, M. and D. Cayman. 2014. Drought and the California Delta- A matter of extremes, San Francisco Estuary & Watershed Science, 1-6.

Ewen, T., et al. 2008a. An extended Pacific North American index from upper air historical data back to 1922, Journal of Climate Vol. 21, 1295–1308.

Ewen, T., et al. 2008b. A monthly upper-air dataset for North America back to 1922. The Monthly Weather Review, 136, 1792–1805.

Feynman, J. and A. Ruzmalkin. 2014. The centennial Gleissberg Cycle and its association with extended minima, Journal of Geophysical Research: Space Physics, 6027- 6041

Gleissberg, W. 1967. Secularly smoothed data on the minima and maxima of sunspot frequency, Solar Physics, Vol. 2,231-233.

Jia X. and J. Ge. 2017. Modulation of the PDO to the relationship between moderate ENSO events and the winter climate over North America, International Journal of Climatology VOL 37, 4275-4287.

Kleppe, J.A., and D. S. Brothers. 2017. Solar forcing of drought detected in snowfall records of the central Sierra Nevada, Western United States, Proceedings 85th Western Snow Conference, 25-38.

Liu, Z., et al. 2017. Pacific North American circulation pattern links external forcing and North American hydroclimatic change over the past millennium, PNAS, Vol. 114, no. 13, 3340-3345.

Mantua, N. and S.R. Hare. 2002. The Pacific Decadal Oscillation, Journal of Oceanography, Vol. 58, 35-44.

Newman, M., et al. 2016. The Pacific Decadal Oscillation, Revisited, Journal of Climate, Vol 29, 4399-4427

Oakley, N. S. and K. T. Redmond. 2014. A climatology of 500-hPa closed lows in the Northeastern Pacific Ocean, 1948-2011, Journal of Applied Meteorology and Climatology, Vol. 53, 1578-1592.

Russel, S., et al. 2014. Improved Historical Temperature and Precipitation Time Series for U.S. Climate Divisions, Journal of Applied Meteorology and Climatology, Vol. 53, No. 5, 1232-1251.

St. George and T.R. Ault. 2011. Is energetic decadal variability a stable feature of the central Pacific Coast's winter climate? Journal of Geophysical Research, Vol. 116, D12102, 1-6.

Svensmark, H., et al. 2017. Increased ionization supports growth of aerosols into cloud condensation nuclei, Nature Communications, 8:2199, 1-9.

Torrence, C. and G. P. Compo. 1998. A practical guide to wavelet analysis, Bulletin of the American Meteorological Society, Vol. 79 No. 4, 61-78.

Yu, F. and G. Luo. 2014. Effect of solar variations on particle formation and cloud condensation nuclei, Environmental Research Letters, Vol. 9 No. 4, 1-7.

Zhang, et al. 1997. ENSO-like interdecadal variability, Journal of Climate, Vol. 10, 1004-1020.